

# Efficient Inverted Planar Perovskite Solar Cells Using Ultraviolet/Ozone-Treated NiO<sub>x</sub> as the Hole Transport Layer

Tun Wang, Dong Ding, Hao Zheng, Xin Wang, Jiayuan Wang, Hong Liu,\*  
and Wenzhong Shen\*

Nickel oxide (NiO<sub>x</sub>) has exhibited great potential as a hole transport layer (HTL) for fabricating efficient and stable perovskite solar cells (PSCs). However, it has been greatly limited by its fabrication and manipulation process. In this work, a simple processing method on an ultrathin electrochemical mesoporous NiO<sub>x</sub> film manipulated by controllable ultraviolet/ozone (UVO) treatment is employed; the duration of UVO treatment on the NiO<sub>x</sub> film significantly affects the photovoltaic properties of the PSCs. When the exposure duration increases, the wettability, electrical conductivity, nonstoichiometry, and valence band energy of the NiO<sub>x</sub> film are improved with varying degrees. Besides, the perovskite grain size, recombination resistance at the perovskite/NiO<sub>x</sub> interface, and build-in potential of the device also increase, resulting in higher short-circuit current density ( $J_{sc}$ ) and open-circuit voltage ( $V_{oc}$ ). Combining these factors together, an optimal exposure time of UVO treatment on the NiO<sub>x</sub> film has been achieved at 5 min, which results in a significantly high performance with an efficiency of 19.67%, large  $V_{oc}$  (>1.1 V), and  $J_{sc}$  (>23 mA cm<sup>-2</sup>). Furthermore, the experimental results are coincide well with simulation results on the different corresponding subjects. Hopefully, this work could facilitate material manipulation toward scalable, high efficiency, and stable solar cells.

## 1. Introduction

The organic–inorganic hybrid perovskite solar cells (PSCs) have attracted huge interests because of their high power conversion efficiency (PCE), simple fabrication process, and low-cost potential.<sup>[1,2]</sup> After a rapid development over the past decade, a certified record has been achieved to over 23%.<sup>[3–5]</sup> Among all configurations, the p-i-n planar structure based on inorganic hole transport layer (HTL) has emerged as a competitive one due to its excellence in low hysteresis and long term stability.<sup>[6–9]</sup> As an important part of the inverted PSCs, the HTL has been often

selected from nonstoichiometric metal oxides (such as CuO<sub>x</sub>,<sup>[10]</sup> MoO<sub>x</sub>,<sup>[11]</sup> and NiO<sub>x</sub><sup>[12]</sup>) for their low cost and tunable opto-electronic properties. NiO<sub>x</sub>, for instance, has been focused in many previous researches with its good energy band matching with perovskite<sup>[12,13]</sup> and shown attractive results such as a highest PCE record of 20.86% in mixed cation PSCs.<sup>[14]</sup> However, like the other candidates, NiO<sub>x</sub> has been normally fabricated either by solution based methods such as spin-coating,<sup>[15]</sup> with less controllability and scalability or vacuum based techniques (such as magnetron sputtering,<sup>[16]</sup> atomic layer deposition (ALD),<sup>[17]</sup> and pulsed laser deposition (PLD)<sup>[18]</sup>) with remarkably high cost and low productivity toward application. To compensate those disadvantages, the electrochemical deposition (ECD) method could be a more suitable option, with which a recent record of 17.0% (with active area ≈0.1084 cm<sup>2</sup>) and 19.2% (with active area ≈0.1 cm<sup>2</sup>) has been achieved by Park et al.<sup>[19]</sup> Nevertheless, as being more and more concerned, the control of oxygen vacancy in this nonstoichiometric NiO<sub>x</sub> has

never been an easy task, whose content and distribution could severely influence the transportability of carriers and thus its photovoltaic performance in devices.<sup>[20]</sup> Some researchers have concerned on the interfacial engineering and proposed to insert transition layer between HTL and perovskite film. However, this process is quite complicated and uncontrollable.<sup>[21,22]</sup> As a routine approach, ultraviolet/ozone (UVO) treatment has been applied in many processes in the fabrication of oxide charge transport layers (such as TiO<sub>2</sub>,<sup>[23]</sup> SnO<sub>2</sub>,<sup>[24]</sup> ZnO,<sup>[25]</sup> and MoO<sub>x</sub><sup>[26]</sup>) in PSCs. Compared to the studies on electron transport layer (ETL) such as SnO<sub>2</sub> and TiO<sub>2</sub>, as a hole transporter, the study on NiO<sub>x</sub> has been focused on different properties, such as valence band, work function, optical gap, while the former ETLs have been mainly studied for their conduction band and surface wettability before perovskite depositing.<sup>[23,27]</sup> Recently, Zhai et al. studied the influence of different annealing temperatures on UVO-treated NiO<sub>x</sub> film, and considered time as constant.<sup>[28]</sup> Furthermore, Wang et al. focused qualitatively on the effect of presence of UVO treatment on the NiAc for preparing polymer solar cells, in which only NiAc under different conditions (with some NiOOH formed after UVO) has been researched.<sup>[29]</sup>

Dr. T. Wang, D. Ding, H. Zheng, X. Wang, J. Wang, Dr. H. Liu,  
Prof. W. Shen  
Key Laboratory of Artificial Structures and Quantum Control (Ministry  
of Education)  
Institute of Solar Energy  
School of Physics and Astronomy  
Shanghai Jiao Tong University  
800 Dongchuan Road, Shanghai 200240, P. R. China  
E-mail: liuhong@sjtu.edu.cn; wzshen@sjtu.edu.cn

DOI: 10.1002/solr.201900045

However, the evolution of the stoichiometry, microstructure and chemical state of electrochemical NiO<sub>x</sub> in difference time stages during the UVO treatment has never been discussed. Besides, the optimal exposure duration of UVO treatment on NiO<sub>x</sub> film for preparing PSCs is still not clear. Therefore, it would be a worth investigating challenge to experimentally manipulate the stoichiometry of NiO<sub>x</sub> as well as its microstructure and morphology.

In this study, we propose a facile strategy to prepare a uniform and highly efficient electrochemically fabricated NiO<sub>x</sub> HTL via a novel controllable ultraviolet/ozone (UVO) treatment. UVO treatment improves p-type property of NiO<sub>x</sub> film, optimizes the HTL/perovskite interface and adjusts the energy level of HTL in the inverted planar PSC with a structure of FTO/NiO<sub>x</sub>/MAPbI<sub>3</sub>/PCBM/BCP/Ag, in which NiO<sub>x</sub> film is firstly deposited by ECD method. We have shown that the stoichiometry of the sample can be effectively controlled by manipulation of the UVO treatment. Based on that, a well balance could be established among the optical transmittance property, wettability, surface morphology, electrical conductivity, optical bandgap and carrier dynamics of the as-prepared NiO<sub>x</sub> materials. Consequently, remarkable enhancement of cell performance has been induced with a PCE of 19.67% ( $V_{OC}$  and  $J_{SC}$  increased from 1.01 V to 1.11 V and from 21.69 mA cm<sup>-2</sup> to 23.41 mA cm<sup>-2</sup>, respectively) for the champion device under optimal duration (5 min) of UVO treatment on NiO<sub>x</sub> HTL, with negligible hysteresis and high stability. In comparison, the PSC device using pristine NiO<sub>x</sub> shows the highest efficiency only 17.32%. To further verify the effect of UVO treatment on the photovoltaic performances of PSCs due to the improved physical and chemical properties of NiO<sub>x</sub> film, the simulation based on Lumerical's optical simulation software of finite-difference time-domain (FDTD) solutions 2017a and electrical simulation solver of DEVICE 2015a have been implemented. The simulated electrical performances of the corresponding PSCs are consistent with our experimental results, and have also revealed that the incident light is more efficiently coupled into the perovskite layer from UVO-treated NiO<sub>x</sub> comparing with the pristine NiO<sub>x</sub> film.

## 2. Results and Discussion

First of all, a thin layer of Ni(OH)<sub>2</sub> was firstly obtained by ECD process and the NiO<sub>x</sub> film can be finally prepared after thermal annealing,<sup>[30]</sup> as indicated by **Figure 1a**. The curve on the bottom represents the X-ray diffraction (XRD) pattern of FTO substrate, which shows very strong characteristic peaks. The curve in the middle corresponds to the unannealed sample, showing two significant diffraction peaks at 33.1° and 38.5° (indicated by diamond marks) which are assigned to the (100) and (011) planes of Ni(OH)<sub>2</sub>, respectively.<sup>[31]</sup> It has been reported that the electrical conduction of NiO<sub>x</sub> transits from n-type to p-type with post-deposition annealing at 200 °C and the optical band gap, refractive index, carrier concentration, mobility and hall coefficient of NiO<sub>x</sub> are varied to some extent with the annealing temperature increasing from 100 to 500 °C.<sup>[32]</sup> Considering the decomposition temperature of Ni(OH)<sub>2</sub> is below 300 °C,<sup>[33]</sup> we post-annealed the samples at 300 °C for 2 h, and a variety of literatures have also demonstrated that 300 °C is indeed the optimal annealing temperature for preparing NiO<sub>x</sub> HTL during

fabrication process of inverted PSCs.<sup>[6–8,34–36]</sup> After thermal annealing at 300 °C for 2 h, these peaks vanished and new peaks appeared at 37.2° and 43.3° (indicated by the star marks) owing to the transformation of Ni(OH)<sub>2</sub> to NiO<sub>x</sub>, which can be assigned to the (111) and (200) planes, respectively,<sup>[37]</sup> well matching with the cubic structure of NiO PDF-#47-1049. The estimated grain size of NiO<sub>x</sub> according to the XRD pattern is 10.3 nm by using Debye-Scherrer equation,<sup>[38]</sup> which is consistent with the previous report.<sup>[39]</sup> The top view scanning electron microscopy (SEM) image of the electrochemically deposited NiO<sub>x</sub> film is shown in **Figure 1b**, indicating the FTO nanograins are totally covered by mesoporous NiO<sub>x</sub> films. The mesoporous film becomes much denser with the increasing deposition time according to the SEM images in the Supporting Information (**Figure S1a–e**, Supporting Information). Besides, the thickness of deposited NiO<sub>x</sub> film can be accurately controlled by adjusting the deposition time,<sup>[40]</sup> and corresponding current density–voltage (*J*–*V*) characterization of PSCs has verified that the optimal ECD deposition time for fabrication of NiO<sub>x</sub> is 90 s (details can be found in **Figure S1** and **S2**, Supporting Information), with constant current density of 0.1 mA cm<sup>-2</sup>.<sup>[19]</sup> The inset of **Figure 1b** illustrates the cross-sectional image of the NiO<sub>x</sub> film prepared under optimal deposition time of 90 s and its thickness is about 40 nm, much thinner than the reported optimal thickness (50–150 nm) by solution-derived spin-coating method.<sup>[13,34,39,41]</sup> Benefiting from the electrochemical deposition method, the FTO grains are fully covered by NiO<sub>x</sub> film even though it is very thin (**Figure S1c**, Supporting Information), thus effectively avoiding direct contact and current leakage between perovskite and conducting substrate. The thinner NiO<sub>x</sub> film can reduce series resistance and introduce less internal crystal boundaries, leading to less recombination in the NiO<sub>x</sub> film.<sup>[42]</sup> The root-mean square (RMS) roughness of prepared mesoporous NiO<sub>x</sub> film is 10.9 nm according to the three-dimensional atomic force microscopy (AFM) image in **Figure 1c**, slightly smaller than that of the bare FTO substrate (**Figure 1d**), with RMS roughness up to 14.3 nm. Noticeably, the simplest solution process to grow perovskite layer is the one-step method, in which the precursors are transformed into crystalline perovskite through fast solvent evaporation during spin-coating and annealing, so the controllability of the crystal growth and film uniformity would become challenging, especially for a rough substrate.<sup>[43]</sup> Therefore the NiO<sub>x</sub> substrate with lower roughness would be beneficial in this case.

As commonly known, UVO treatment has been an effective way to modify the surface and electrical properties of thin films.<sup>[20,23,26]</sup> However, the exact process and influence on the nonstoichiometric materials has seldom been studied, thus we have carried out the UVO treatment on the as-prepared samples with different times. Firstly, the physical characterization has been presented in **Figure 2**. **Figure 2a** shows the optical transmittance spectra of the prepared NiO<sub>x</sub> film deposited on FTO substrate with different times of UVO treatment. All the deposited NiO<sub>x</sub> films have displayed high transmittance around 85% over a broad spectral range (400–800 nm), almost the same with bare FTO substrate. Such a high transparency would be a good preliminary condition for PSCs. The wettability measurement has shown drastic change of surface tension with the UVO treatment. As shown in **Figure 2b**, the contact angle of the

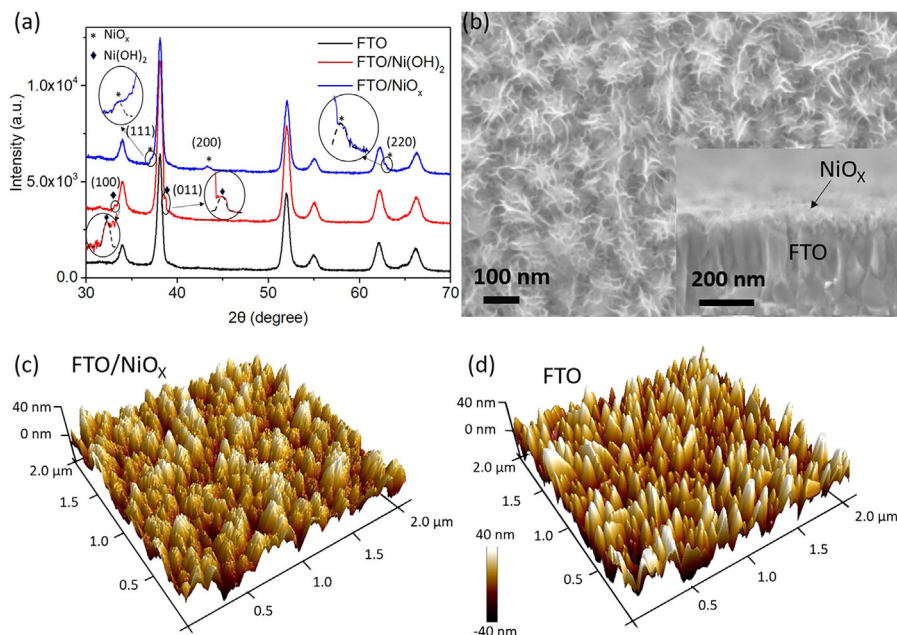


**Figure 1.** a) Comparison of the XRD pattern of FTO, Ni(OH)<sub>2</sub> and NiO<sub>x</sub>. b) Top-view SEM image of prepared NiO<sub>x</sub> mesoporous film on FTO substrate. The inset shows the cross-sectional SEM image of the deposited NiO<sub>x</sub> film under optimal deposition condition. Three-dimensional AFM images of (c) NiO<sub>x</sub> film deposited on FTO and (d) bare FTO substrate.

control sample without UVO treatment was 45.6° and dramatically decreased to around 25° after UVO exposure with different times. The slight recovery of hydrophobicity with longer UVO exposure time is probably attributed to loss of low

molecular weight organic material that has been created on the surface during UVO treatment and reorientation of side groups on the molecules due to the burying of newly formed polar groups in the exposure region.<sup>[44,45]</sup> The smallest contact angle

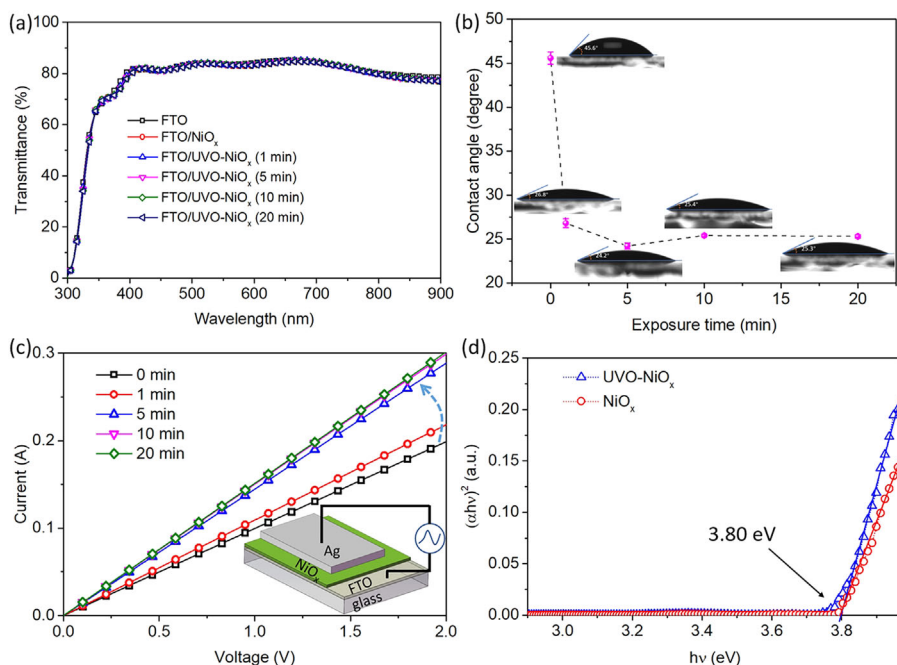


**Figure 2.** Physical properties of NiO<sub>x</sub> processed under different conditions: a) Optical transmission spectra of bare FTO substrate and deposited NiO<sub>x</sub> films with different UVO exposure times. b) Contact angles of a water droplet on NiO<sub>x</sub> surfaces as a function of UVO exposure time. c) I–V curves for initial and UVO-treated NiO<sub>x</sub> films with different exposure times based on FTO/NiO<sub>x</sub>/Ag structure. d) Tauc plots for the NiO<sub>x</sub> films with and without UVO treatment. For clarity, FTO/UVO-NiO<sub>x</sub> and FTO/NiO<sub>x</sub> stand for the sample with and without UVO treatment, respectively.

24.2° is obtained by exposure under UVO for 5 min, which facilitates the formation of a more uniform perovskite layer.<sup>[46,47]</sup> The current–voltage (*I*–*V*) characteristics have been measured under dark condition to determine the effect of UVO treatment on the electrical conductivity of the NiO<sub>x</sub> film (Figure 2c). The linear *I*–*V* characteristics exhibit perfect ohmic contact between p-type NiO<sub>x</sub> and Ag electrode. As we know, the electrical conductivity is proportional to the tangent of the *I*–*V* curve. Hence, the electrical conductivity of the NiO<sub>x</sub> film after UVO treatment has been significantly improved compared to the pristine NiO<sub>x</sub> film without UVO treatment, and gradually increased with longer exposure time of the UVO radiation (Figure S3, Supporting Information).<sup>[48]</sup> The conductivities are estimated to be  $1.99 \times 10^{-6} \text{ S cm}^{-1}$  (0 min),  $2.19 \times 10^{-6} \text{ S cm}^{-1}$  (1 min),  $2.89 \times 10^{-6} \text{ S cm}^{-1}$  (5 min),  $3.00 \times 10^{-6} \text{ S cm}^{-1}$  (10 min), and  $3.01 \times 10^{-6} \text{ S cm}^{-1}$  (20 min), respectively. This result is roughly consistent with the previous literature,<sup>[20]</sup> in which the electrical conductivity rose to more than one order of magnitude higher after the NiO<sub>x</sub> film was treated by UVO for 10 min. Furthermore, we have derived the optical bandgap of the samples from the Tauc plots in Figure 2d, in which  $(\alpha h\nu)^2$  is plotted as a function of *hν* from previous absorption spectra, with  $\alpha$ , *h*, and  $\nu$  representing the absorption coefficient, Planck constant, and light frequency, respectively. The estimated optical gaps are both approximately 3.80 eV, quite consistent with the reported values.<sup>[42,49]</sup> According to this study, the UVO treatment on the bandgap of NiO<sub>x</sub> has been not significant.

Secondly, high energy photons could also influence the oxidation state and crystalline situation in the oxides.<sup>[20,50]</sup> Therefore the chemical and microstructural properties of the objects have been further investigated, as shown in **Figure 3**. Figure 3a and b illustrate the high-resolution X-ray photoelectron

spectroscopy (XPS) spectra of the Ni 2p<sub>3/2</sub> and O 1s core levels of the prepared NiO<sub>x</sub> films, respectively. The black scatters denote the pristine NiO<sub>x</sub> without UVO treatment and the colored scatters represent the NiO<sub>x</sub> films exposed by UVO versus different time. The solid and dashed lines in both Ni 2p<sub>3/2</sub> and O 1s core levels are the fitted components that corresponding to different chemical states.<sup>[14,17,51]</sup> For the NiO<sub>x</sub> without UVO treatment, the peak at 860.9 eV in the Ni 2p<sub>3/2</sub> spectrum is ascribed to the shakeup process of the NiO structure.<sup>[39,42,52]</sup> Other three distinct peaks are corresponding to the presence of NiO in the cubic rock-salt structure<sup>[52]</sup> (853.8 eV in Ni 2p<sub>3/2</sub> and 529.2 eV in O 1s), Ni<sub>2</sub>O<sub>3</sub> in the hexagonal crystal structure<sup>[53]</sup> (855.5 eV in Ni 2p<sub>3/2</sub> and 530.9 eV in O 1s) and NiOOH (856.5 eV in Ni 2p<sub>3/2</sub> and 531.5 eV in O 1s) due to some residual hydroxide,<sup>[54]</sup> respectively. Comparing the XPS spectra of the NiO<sub>x</sub> under different conditions together, we find that Ni<sup>3+</sup> state has been gradually outnumbering the Ni<sup>2+</sup> state with increasing time (can be found in Figure S4a in the supporting information). This change has clearly indicated a continuous stoichiometry (O/Ni ratio) transformation versus time (Figure S4b, Supporting Information), which is consistent with the formation of Ni vacancies.<sup>[20]</sup> More importantly, it has also indicated the significant controllability of the *x* value in the NiO<sub>x</sub> by the UVO treatment. Furthermore, the whole spectrum appears to shift toward higher binding energy with the increasing time of UVO exposure (Figure S5, Supporting Information). For instance, the corresponding peaks of NiO, Ni<sub>2</sub>O<sub>3</sub>, and NiOOH of the NiO<sub>x</sub> film by UVO treatment for 20 min, plotted by the olive dashed curves in Ni 2p<sub>3/2</sub> spectrum (Figure 3a), eventually increase to 854.1 eV, 855.7 eV, and 857.4 eV, respectively. In terms of the O 1s spectrum (Figure 3b), the corresponding peaks also shift to higher binding energy after being treated for 20 min,

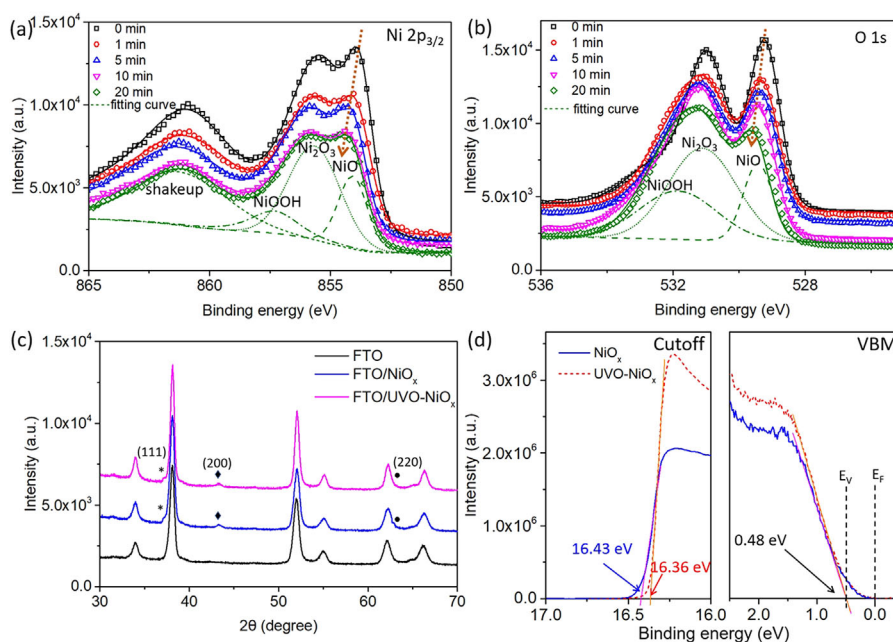


**Figure 3.** XPS spectra of (a) Ni 2p<sub>3/2</sub> and (b) O 1s core levels of the NiO<sub>x</sub> HTL exposed by UVO with different times. The dashed curves indicate Gaussian fitting peaks of the NiO<sub>x</sub> film by UVO treatment of 20 min. c) Comparison of the XRD pattern of NiO<sub>x</sub> film with and without UVO treatment. d) UPS spectra of the NiO<sub>x</sub> and UVO-NiO<sub>x</sub> films deposited on FTO substrate.

the binding energies are 529.5 eV, 531.2 eV, and 532.5 eV, respectively. Such a total shift has indicated higher positive oxidation state with the exposure lasted, and therefore less oxygen vacancies. In addition to UVO treatment, annealing temperature also exhibits the ability to adjust the stoichiometry of NiO<sub>x</sub>. However, such change seems quite small, as reported by Mancieru that the O/Ni ratio increases from 1.010 to 1.016 with the annealing temperature increasing from 350 to 600 °C.<sup>[55]</sup> In this paper, we just focus the effect of UVO treatment on NiO<sub>x</sub> film under optimal annealing temperature.

As shown in Figure 3c, the microstructure change in the samples has been analyzed by XRD, where no significant difference could be detected between the XRD peaks of the UVO-treated and control sample, indicating that the influence of UVO treatment on the microstructure of the NiO<sub>x</sub> has been trivial. Moreover, the energy band alignment between the light absorber and charge transport layers plays a significant role in the extraction/transfer process of the photo-induced carriers. Hence ultraviolet photoelectron spectroscopy (UPS) has been carried out to check the energy levels of the prepared NiO<sub>x</sub> films. As shown in Figure 3d, the photoemission cutoff spectra (in the left panel) indicates that the work function ( $W_F$ ) of prepared NiO<sub>x</sub> film has increased from 4.79 eV to 4.86 eV after UVO treatment, where  $W_F$  can be calculated by the formula  $W_F = h\nu (21.22 \text{ eV}) - E_{\text{cutoff}}$ . The right panel of Figure 3d shows the difference between the valence band and Fermi level ( $E_V - E_F$ ), which has been 0.48 eV for both situations. The valence band maximum (VBM) of the prepared NiO<sub>x</sub> film has shifted from 5.27 eV to 5.34 eV after UVO treatment. The deeper VBM of UVO-NiO<sub>x</sub> film can closely match that of the perovskite layer to minimize the energy misalignment for the holes extraction, which shows great potential to induce higher  $V_{OC}$  of the PSCs.<sup>[16,56]</sup>

Finally, to investigate the NiO<sub>x</sub> samples in real applications, PSCs have been fabricated based on them. Firstly, perovskite film has been deposited on the UVO-exposed NiO<sub>x</sub> film in a glovebox filled with nitrogen by one-step spin-coating process. As shown in Figure 4a and b, the resulting perovskite layers are dense and uniform for the samples with or without UVO treatment. However, the grain size of the UVO-treated NiO<sub>x</sub> has been significantly larger than the untreated control sample, as shown in Figure 4c, which could hopefully facilitate the transport and collection of photogenerated carriers because of less grain boundaries.<sup>[57,58]</sup> The increase in perovskite crystal grain size could be ascribed to the smaller number of nuclei formed on UVO-treated NiO<sub>x</sub> surface because of lowered surface energy.<sup>[59,60]</sup> Besides, the UVO treatment improves the work function of prepared NiO<sub>x</sub> film, which is beneficial to the formation of ohmic contact between NiO<sub>x</sub> film and perovskite precursor materials.<sup>[29]</sup> To study the effect of UVO treatment on carrier dynamics of NiO<sub>x</sub> film, we have investigated interfacial charge-carrier characteristics that influences photovoltaic performances of NiO<sub>x</sub>-based PSCs. Steady-state photoluminescence (PL) and time-resolved photoluminescence (TRPL) measurements were carried out to study the efficiency of charge extraction. As illustrated in Figure 4d, FTO/MAPbI<sub>3</sub> structure displays a strong perovskite emission signal nearly at 764.6 nm and the UVO-NiO<sub>x</sub> film exhibits more efficient PL quenching for MAPbI<sub>3</sub> layer than the pristine NiO<sub>x</sub> film, suggesting enhanced hole extraction ability and transport efficiency from perovskite

layer after UVO treatment. The TRPL spectra shown in Figure 4e demonstrates that the UVO treatment successfully accelerates the hole-extraction process from the perovskite layer to the NiO<sub>x</sub> HTL, which is in accordance with the steady PL spectra. The TRPL decay curves were fitted to a bi-exponential Equation (1).<sup>[35]</sup>

$$I(t) = A_1 \exp\left(-\frac{t-t_0}{\tau_1}\right) + A_2 \exp\left(-\frac{t-t_0}{\tau_2}\right) \quad (1)$$

where  $t_0$  is the start time of decay process,  $\tau_1$  and  $\tau_2$  represent the first and second order decay times,  $A_1$  and  $A_2$  are weighting coefficients of each decay channel. In general, the fast decay component ( $\tau_1$ ) is due to the quenching of charge carriers at the HTL/perovskite interface, and the slow decay component ( $\tau_2$ ) is attributed to the radiative recombination of free charge carriers.<sup>[61]</sup> The average decay time ( $\tau_a$ ) can be estimated from the Equation (2).<sup>[62]</sup>

$$\tau_a = \frac{\sum A_n \tau_n^2}{\sum A_n \tau_n} \quad (2)$$

The fitted parameters are summarized in Table S1. Notably, the average decay time of MAPbI<sub>3</sub> coated on FTO substrate is 10.5 ns. The structure of FTO/UVO-NiO<sub>x</sub>/MAPbI<sub>3</sub> exhibits a  $\tau_a$  of 4.7 ns, which is much smaller than 7.8 ns of the control sample (FTO/NiO<sub>x</sub>/MAPbI<sub>3</sub>), suggesting a faster hole extraction from the perovskite layer to NiO<sub>x</sub> film with UVO treatment. The large grain size provides greater PL intensity and longer carriers lifetime (TRPL) according to some published literatures.<sup>[63,64]</sup> However, there's also another factor that influence these properties, i.e., the charge transfer from the perovskite to the substrate, which could be induced by charge collection and transport efficiencies.<sup>[34]</sup> It means, lower PL intensity and faster PL decay could be induced by better charge separation and extraction at perovskite/HTL interface.<sup>[59,65]</sup> In this paper, it seems that the improved charge transfer at interface dominates the PL intensity and decay time. The efficient hole transfer significantly contributes to the high  $J_{SC}$  and  $V_{OC}$  values for the NiO<sub>x</sub>-based PSCs. What's more, according to the optical bandgap (Figure 2d), work function and VBM edge (Figure 3d) of prepared NiO<sub>x</sub> and UVO-NiO<sub>x</sub> films, the energy band diagram of prepared PSC device is described in Figure 4f. The energy levels of NiO<sub>x</sub>, perovskite, PCBM, and BCP are well aligned against vacuum. Especially, the smaller VBM difference between UVO-NiO<sub>x</sub> and perovskite layers signifies better hole extraction property comparing with that of the pristine NiO<sub>x</sub> film. The thin BCP layer is believed to work as a hole-blocking layer, which can effectively prevent the recombination of photo-induced carriers and improve the fill factor (FF).<sup>[8,66]</sup>

Afterwards, Ag electrodes have been integrated onto perovskites, forming a structure of FTO/NiO<sub>x</sub>/CH<sub>3</sub>NH<sub>3</sub>PbI<sub>3</sub>/PCBM/BCP/Ag for the PSCs, as illustrated in Figure 5a. The Cross-sectional SEM image of a typical device based on UVO-treated NiO<sub>x</sub> (Figure 5b) has indicated uniform layer formation and quite regular interfacial condition, which shows better coverage of perovskite layer than the device based on pristine NiO<sub>x</sub> film (Figure 5c). The estimated thickness of perovskite layer is approximately 390 nm, close to its average grain size,

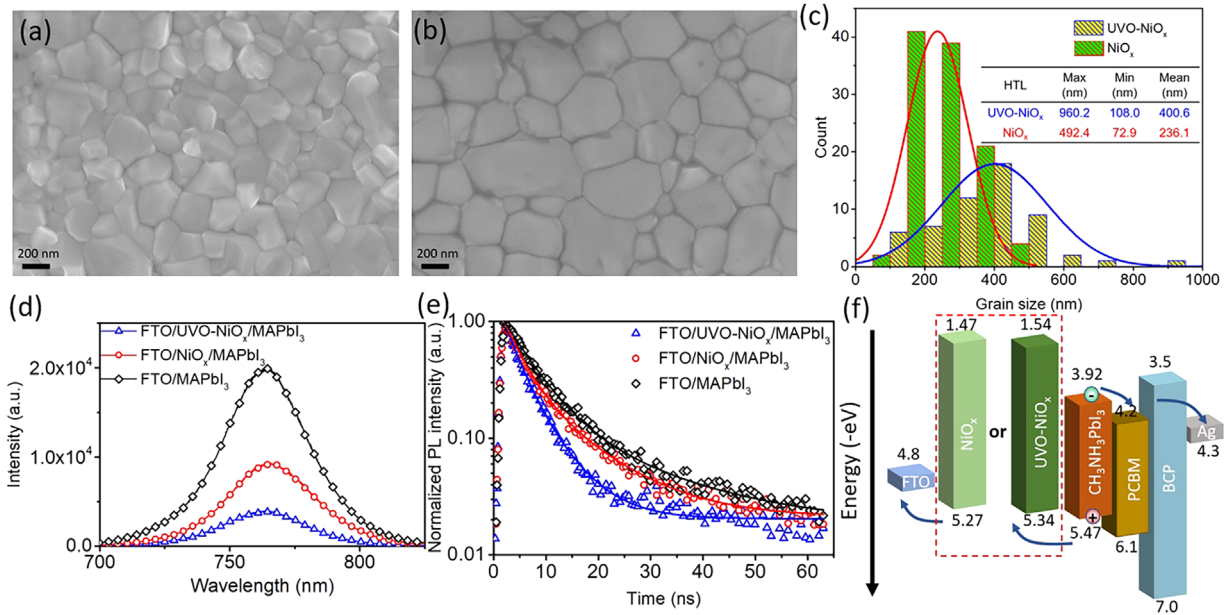


**Figure 4.** Top view SEM image of the perovskite film coated on the NiO<sub>x</sub> film (a) without and (b) with UVO exposure. c) Perovskite grain size distribution histogram of NiO<sub>x</sub>-based device with and without UVO exposure. d) Steady-state and (e) time-resolved photoluminescence spectra of the perovskite film deposited on bare FTO substrate, pristine NiO<sub>x</sub>, and UVO-NiO<sub>x</sub>. f) Schematic representation of the energy band diagram for the PSC device.

which could enhance its photovoltaic performance since the photo-induced carriers can be more easily transported and extracted through one perovskite grain,<sup>[67]</sup> while it is still thick enough for the light absorption.<sup>[9]</sup> The photovoltaic performance of the PSCs with NiO<sub>x</sub> under different conditions has been

studied in details. The optimal *J-V* curves are displayed in Figure 5d, which have been measured under AM 1.5 G simulated sunlight (100 mW cm<sup>-2</sup>). The control device without UVO treatment exhibits a PCE of 17.32%, with a *V*<sub>OC</sub> of 1.01 V, a *J*<sub>SC</sub> of 21.69 mA cm<sup>-2</sup> and an FF of 78.70%. Amazingly, the

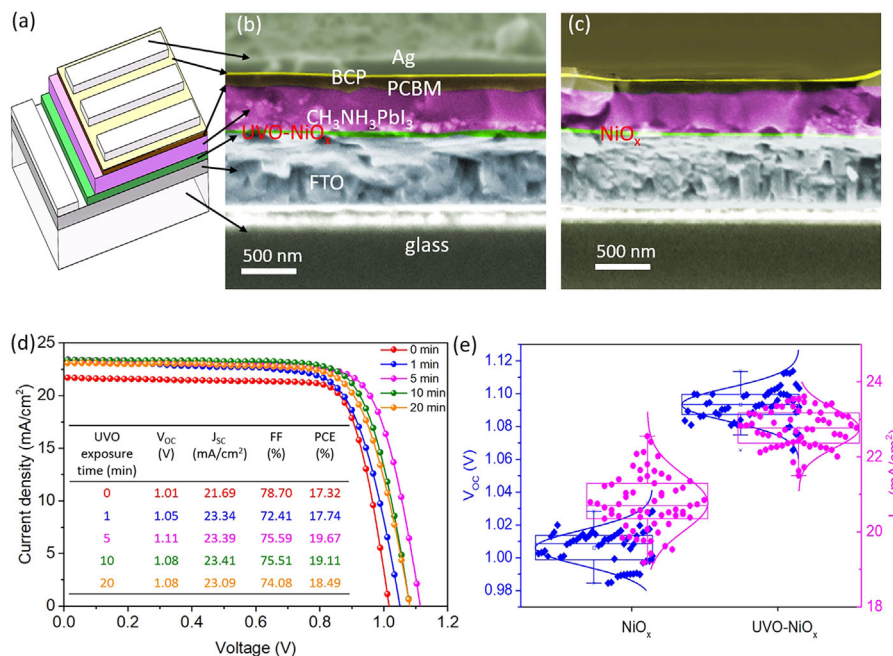


**Figure 5.** a) Three-dimensional schematic diagram of the inverted architecture. False color cross-sectional SEM image of the perovskite solar cell based on (b) UVO-treated NiO<sub>x</sub> and (c) pristine NiO<sub>x</sub>. d) *J-V* curves of optimal PSC devices based on UVO-treated NiO<sub>x</sub> HTL with different exposure times. (e) Statistics of *V*<sub>OC</sub> and *J*<sub>SC</sub> for NiO<sub>x</sub>-based PSCs with and without UVO treatment.

fabricated PSC devices have exhibited greatly improved  $V_{OC}$  and  $J_{SC}$  after UVO treatment on the  $NiO_x$  films. On one hand, the  $J_{SC}$  of all PSCs based on UVO- $NiO_x$  has been larger than  $23\text{ mA cm}^{-2}$ , at least 7.8% higher than that of the control device. The optimal  $J_{SC}$  can be up to  $23.41\text{ mA cm}^{-2}$ , as far as we know, which is comparable to the published record ( $24.19\text{ mA cm}^{-2}$ ) in pure  $MAPbI_3$  system,<sup>[68]</sup> but still shows significant gap to the theoretical limit of  $MAPbI_3$ -based PSCs ( $26.46\text{ mA cm}^{-2}$ ).<sup>[69,70]</sup> On the other hand, the  $V_{OC}$  increment is related to the UVO exposure time. The optimal  $V_{OC}$  increases to 1.05 V, 1.11 V, 1.08 V, and 1.08 V with UVO exposure time at 1 min, 5 min, 10 min, and 20 min, thus yielding an optimal PCE of 17.74%, 19.67%, 19.11%, and 18.49%, respectively. The low performance for the control device without UVO treatment should have been caused by small  $J_{SC}$  and  $V_{OC}$ , which is related to low carrier mobility and high Fermi energy offset between  $NiO_x$  and perovskite.<sup>[16,61]</sup> In comparison, the PSCs based on  $NiO_x$  HTL exposed by UVO for 5 min exhibit much better performance. Figure 5e presents the statistics of photovoltaic parameters  $V_{OC}$  and  $J_{SC}$  for over 50 devices based on pristine  $NiO_x$  and UVO- $NiO_x$  HTL, respectively. The larger  $J_{SC}$  and higher  $V_{OC}$  could be attributed to the higher hole conductivity in the HTL,<sup>[71]</sup> less defects at HTL/perovskite interface and narrower offset of the valence band between  $NiO_x$  and perovskite after appropriate UVO exposure,<sup>[72]</sup> respectively. What's more, as normally known for PSCs, the hysteresis of  $J$ - $V$  characteristics has been an important factor that could deteriorate the stability of the cell output.<sup>[73]</sup>

As shown in Figure 6a, UVO- $NiO_x$ -based PSCs and control device have both exhibited negligible hysteresis, where the

**Table 1.** Photovoltaic parameters of the PSCs based on  $NiO_x$  and UVO- $NiO_x$  HTL.

Sample	Scan direction	$V_{OC}$ [V]	$J_{SC}$ [ $\text{mA cm}^{-2}$ ]	FF [%]	PCE [%]
$NiO_x$	Reverse	1.01	21.69	78.70	17.32
	Forward	1.02	21.48	78.10	17.05
UVO- $NiO_x$	Reverse	1.11	23.39	75.59	19.67
	Forward	1.11	23.30	75.18	19.48

champion devices have shown PCE of 19.67%, 17.32% for the backward scanning and 19.48%, 17.05% for the forward scanning, respectively. Detail parameters are listed in Table 1. For further understand the enhancement of the photovoltaic performance, the space-charge limited current method was employed to examine the defect states at perovskite/HTL interface. The trap-state density ( $n_{trap}$ ) can be calculated according to Equation (3).<sup>[21]</sup>

$$n_{trap} = \frac{2\epsilon\epsilon_0 V_{TFL}}{eL^2} \quad (3)$$

where  $\epsilon$  and  $\epsilon_0$  are the relative dielectric constant of perovskite (6.5)<sup>[74]</sup> and vacuum, respectively.  $e$  is elementary charge, and  $L$  is the thickness of the film between two electrodes ( $\approx 500\text{ nm}$ ).  $V_{TFL}$  is the trap-filling limited (TFL) voltage, which could be derived from the  $J$ - $V$  curves under dark condition, as shown in Figure 6b. The  $V_{TFL}$  of the hole-only devices (FTO/ $NiO_x$ /perovskite/Ag) based on UVO-treated  $NiO_x$  and pristine  $NiO_x$  are

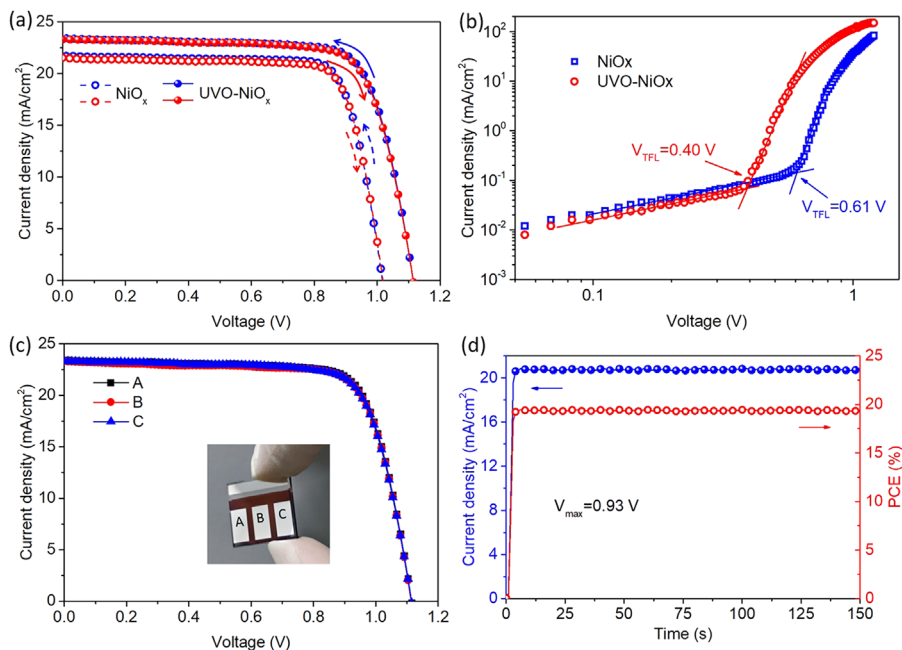


**Figure 6.** a)  $J$ - $V$  curves of champion PSC devices based on pristine and UVO-treated  $NiO_x$ , which were measured under different scan directions, showing negligible hysteresis. b) Dark  $J$ - $V$  measurement of the hole-only devices. c)  $J$ - $V$  curves measured from different positions with an active area of  $0.25\text{ cm}^2$ , the inset indicates the real image of prepared PSC device. d) Steady-state photocurrent of the champion device measured at a bias voltage (0.93 V) near the maximum power point and respective calculated PCE.

0.40 and 0.61 V, respectively. As a result, the calculated  $n_{\text{trap}}$  decreased from  $1.76 \times 10^{15} \text{ cm}^{-3}$  for  $\text{NiO}_x/\text{perovskite}$  to  $1.15 \times 10^{15} \text{ cm}^{-3}$  for the UVO- $\text{NiO}_x/\text{perovskite}$ , which demonstrates a reduced trap recombination at HTL/perovskite interface for the UVO-treated  $\text{NiO}_x$ . Compared to the spin-coating method, the  $\text{NiO}_x$  film fabricated by ECD method is relatively more uniform and is more scalable for large area devices with absence of mechanical fabrication procedure.<sup>[19]</sup> Moreover, the devices have all presented good uniformity without edge influence (Figure 6c), where  $J-V$  characteristics have been measured at different positions. This has proved significant excellence of this method in the scalability of cells, which is an important factor for real application of devices. As shown in Figure 6d, the photocal of the champion device by applying a bias voltage at the maximum output point (0.93 V) was quickly stabilized after the light was turned on, and the stabilized PCE values were very close to the result from the  $J-V$  measurement, both of which support the negligible hysteresis behavior of our PSCs.

Furthermore, the external quantum efficiency (EQE) spectra in Figure 7a has illustrated the detail of the improved photovoltaic performance of UVO- $\text{NiO}_x$  based PSCs from the spectroscopic response, where the EQE has been gradually enhanced in 350–500 nm and 600–700 nm regions with the increasing exposure time of UVO treatment on  $\text{NiO}_x$  film. The spectrum has shown a broad plateau around 90% in the range of 350–750 nm, which is consistent with previous literatures, where the maximum values are all above 90% for  $\text{MAPbI}_3$ -based PSCs.<sup>[43,75–78]</sup> The integrated  $J_{\text{SC}}$  of the champion device can be up to  $22.55 \text{ mA cm}^{-2}$ , consisting with the measured  $J_{\text{SC}}$  of

$23.39 \text{ mA cm}^{-2}$  by the  $J-V$  measurements. The enhancement of  $J_{\text{SC}}$  is partly attributed to improved electrical conductivity of  $\text{NiO}_x$  HTL and better crystallinity of perovskite grown on UVO-treated  $\text{NiO}_x$  film.<sup>[79,80]</sup> The improved carrier transport and extraction abilities can also efficiently improve the EQE values by some recent reports.<sup>[14,75,81]</sup> Besides, interface condition may play a crucial role according to previous discussion. To investigate that, the electrical impedance spectroscopy (EIS) has been also performed, which could provide more insight into the charge transport process and contact resistance information.<sup>[67]</sup> It is well known that in the Nyquist plot, the high-frequency part (arc at the left) corresponds to the transfer resistance ( $R_{\text{tr}}$ ) and the low-frequency part (arc at the right) corresponds to the recombination resistance ( $R_{\text{rec}}$ ).<sup>[61,82]</sup> However, the arc at the high frequency region (left side of the curve) has almost vanished and cannot be observed in the Nyquist plots shown in Figure 7b, which indicates a large conductivity in the hole transport layer. The only one semicircle will then be more likely related to the recombination processes.<sup>[66]</sup> It means that the  $R_{\text{rec}}$  of the UVO- $\text{NiO}_x$  based PSCs is much higher than that of the control sample without UVO treatment, i.e., a decreased recombination at the interfaces.<sup>[83]</sup> The highest  $R_{\text{rec}}$  is obtained at 5 min of UVO treatment, which is consistent with the above discussion. Furthermore, the junction properties at the HTL/perovskite interface was also investigated by capacitance–voltage ( $C-V$ ) characterizations, which were conducted under dark condition. As shown in Figure S6, Supporting Information, the Mott-Schottky impedance analysis plotted by  $C^{-2}$  vs. voltage indicates larger built-in potential ( $V_{\text{bi}}$ ) for UVO- $\text{NiO}_x$ -based perovskite device (1.03 V) comparing with  $\text{NiO}_x$ -based perovskite (0.89 V),

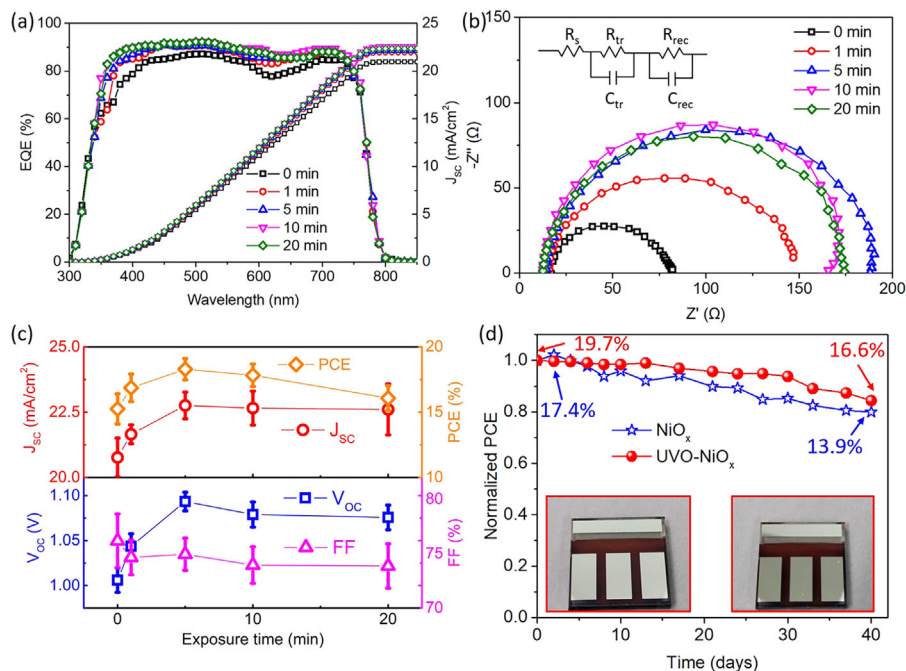


**Figure 7.** a) EQE and integrated  $J_{\text{SC}}$  spectra, (b) EIS Nyquist plots and (c) photovoltaic parameters ( $V_{\text{OC}}$ ,  $J_{\text{SC}}$ , FF, and PCE) distributions of perovskite devices based on UVO-treated  $\text{NiO}_x$  with different UVO exposure time. The inset shows equivalent circuit by Nyquist fitting. (d) Normalized PCE of PSC devices based on pristine and UVO-treated  $\text{NiO}_x$  films as a function of storage time. The insets are the real device images at the start and end of the long-term storage.

where  $V_{bi}$  can be estimated from the x-intercept of fitting line from the Mott-Schottky plot. The increased  $V_{bi}$  could accelerate charge dissociation and avoid charge accumulation at HTL/perovskite interface,<sup>[17,84,85]</sup> which can also attribute to higher  $V_{OC}$  and this result is consistent with the above discussion about EIS measurement. Therefore, the much larger  $V_{OC}$  of PSCs based on UVO-treated  $NiO_x$  is the result of multiple factors, including the higher hole conductivity in the HTL, the improvement of the crystallinity and surface coverage of the perovskite films, the reduced defects at HTL/perovskite interface, and the narrowed offset of the valence band between  $NiO_x$  and perovskite film. Figure 7c exhibits the photovoltaic performance distribution of PSCs based on different exposure time of UVO treatment on  $NiO_x$  HTL. It can be observed that the prepared PSCs based on pristine  $NiO_x$  display an average  $J_{SC}$  of  $20.77 \text{ mA cm}^{-2}$ , a  $V_{OC}$  of 1.01 V and a PCE of 76.19%, resulting in a relatively low average PCE of 15.26%. When increasing the exposure time of UVO treatment to 5 min, the average  $J_{SC}$  and  $V_{OC}$  of PSCs are increased to  $22.76 \text{ mA cm}^{-2}$  and 1.09 V, respectively, both of which are much higher than that of the PSCs based on UVO-treated  $NiO_x$  with the other three exposure times. Note that the FF of the devices with UVO-treated  $NiO_x$  under different durations of UVO exposure are approximately equal, but smaller than that of the pristine  $NiO_x$ , which may be ascribed to the imbalance of the electron and hole mobilities.<sup>[86,87]</sup> As a consequence, the champion PCE is achieved with UVO treatment on  $NiO_x$  HTL for 5 min. Moreover, the devices with UVO exposure for 5 min perform smallest error bars of photovoltaic performance comparing with other different UVO treatment conditions, demonstrating excellent reproducibility and reliability of the planar-type PSC. In addition to the high photovoltaic efficiency, the durability of the PSCs for long-term application is another major concern. We therefore carried out the long-term stability of fabricated PSCs without encapsulation in inert environment ( $H_2O < 1 \text{ ppm}$  and  $O_2 < 0.1 \text{ ppm}$ ) at room temperature and the  $J-V$  curves were periodically measured to extract the photovoltaic parameters. As shown in Figure 7d, the control device based on pristine  $NiO_x$  HTL has retained around 80% of its initial performance after 40 days

storage, which is comparable with the reported  $NiO_x$ -based devices,<sup>[34,35]</sup> while the resulting UVO- $NiO_x$  based PSC has maintained 84% of its initial efficiency and shown higher long-term stability. The insets of Figure 7d are the real images of the same PSC device based on UVO- $NiO_x$  HTL before and after long-term storage, showing high stability without obvious deterioration. Such improvement of long-term stability could possibly be due to certain passivation effect with less oxygen vacancies compared to the untreated sample and the development of morphological defects at UVO- $NiO_x$ /perovskite interface. A future improvement in the stability of PSCs without sacrificing PCE could be implemented using inorganic perovskite layer and replacing the PCBM with metal oxide charge transport materials.<sup>[6,34]</sup>

To further validate the impact of UVO-treated  $NiO_x$  HTL on the performance of the PSCs with inverted p-i-n planar configuration, Lumerical's FDTD and DEVICE have been deployed to simulate optical-field-intensity distributions in the interfaces and detailed photovoltaic parameters ( $V_{OC}$ ,  $J_{SC}$ , FF, PCE), respectively. The values of work function and electrical conductivity of  $NiO_x$  layer have been determined by our experimental results, while other parameters (such as energy bandgap, carrier mobility, refractive index and defect density of other used materials)<sup>[74,88–90]</sup> have been extracted from published literatures.<sup>[74,88–90]</sup> Figure 7a and b illustrate the optical field distributions with a wavelength of 650 nm in the structures of FTO/ $NiO_x$ /MAPbI<sub>3</sub> and FTO/UVO- $NiO_x$ /MAPbI<sub>3</sub>, respectively. The wavy lines are introduced as interfaces to distinguish different layers with its amplitude and periodicity standing for the roughness. Corresponding to the larger grain size of perovskite layer deposited on UVO- $NiO_x$  (Figure 4), the wavy line representing UVO- $NiO_x$ /MAPbI<sub>3</sub> interface has exhibited relatively longer periodicity than that for the  $NiO_x$ /MAPbI<sub>3</sub> interface. Apparently, as shown in Figure 8a, the light field in MAPbI<sub>3</sub> layer is rather weak, while after UVO treatment on  $NiO_x$  HTL, the stronger optical-field-intensity is observed in the perovskite layer (Figure 8b). This is probably due to the larger perovskite grain size effectively combine with the UVO- $NiO_x$  HTL, which enables the incident light can be efficiently coupled

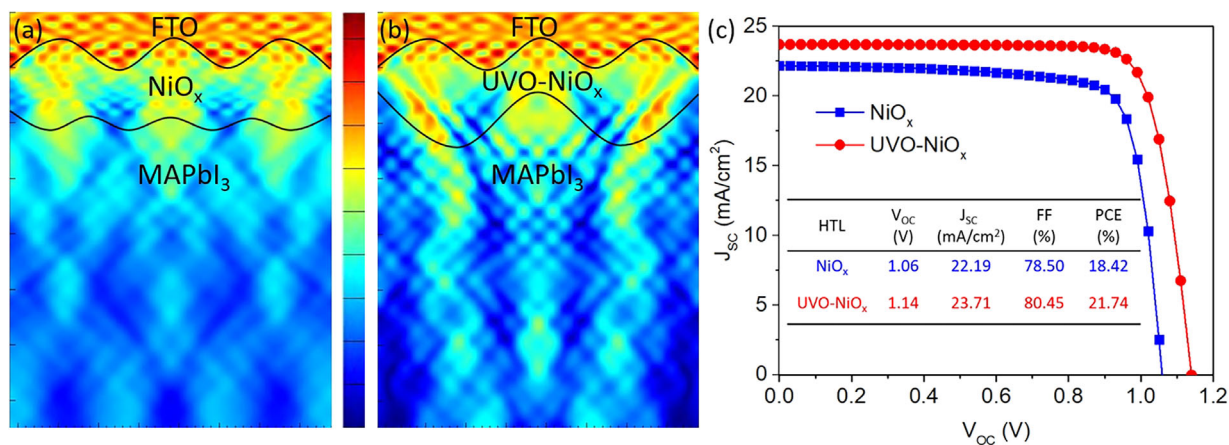


**Figure 8.** Light field distributions in the interfaces of (a) FTO/ $NiO_x$ /MAPbI<sub>3</sub> and (b) FTO/UVO- $NiO_x$ /MAPbI<sub>3</sub>. c) Simulated  $J-V$  curves of PSCs based on  $NiO_x$  HTL with and without UVO treatment.

into the light absorber layer, thus significantly improve the performances. In addition, the improved work function and electrical conductivity of the HTL after UVO treatment have also contributed to efficiently enhancing  $J_{SC}$  and  $V_{OC}$  of prepared PSCs.<sup>[56]</sup> The simulated  $J$ - $V$  curves of PSCs based on  $NiO_x$  and UVO- $NiO_x$  layers are plotted in Figure 8c, where the inset lists the corresponding photovoltaic parameters. The performances have all been enhanced for UVO- $NiO_x$ -based PSCs comparing with the control devices based on  $NiO_x$  HTL. For example, the  $V_{OC}$  increases from 1.06 to 1.14 V, and the corresponding champion PCE increases from 18.42% to 21.74%. Ignoring environmental and test deviations, the simulation results have been well consistent with our experimental results (Figure 5d), revealing meaningful work on understanding the positive influence of UVO-treated  $NiO_x$  layer for inverted PSC devices.

### 3. Conclusions

In summary, we have demonstrated a controllable approach to form high-quality mesoporous  $NiO_x$  film as HTL for efficient PSCs through UVO treatment and ECD technique. The UVO treatment increases the surface wettability, electrical conductivity, and work function of the prepared  $NiO_x$  film, which benefits for good coverage of perovskite layer, leading to efficient extraction of photogenerated holes from the light absorber layer and low interfacial recombination due to the large grain size of perovskite. As a result, the fabricated devices based on UVO-treated  $NiO_x$  film exhibit the highest PCE of 19.67%, with a  $J_{SC}$  of 23.39 mA cm<sup>-2</sup>, a  $V_{OC}$  of 1.11 V, and an FF of 75.59% with good reproducibility and no obvious hysteresis. Comparing with initial  $NiO_x$ -based PSCs, the devices based on UVO-treated  $NiO_x$  film exhibit higher photovoltaic performance, and importantly, it also shows better stability. Further FDTD simulation verifies our experimental results. This study offers a novel strategy to optimize the surface of  $NiO_x$  HTL for designing high-performance PSCs and also paves the way toward commercial and scalable manufacturing of PSCs.

### 4. Experimental Section

**Materials:** The patterned fluorine-doped tin oxide (FTO)-coated glass substrates were purchased from Shanghai MaterWin New Materials Co., Ltd, China. Lead iodide ( $PbI_2$ , 99.9%), methylammonium iodide ( $CH_3NH_3I$ , 99.5%), phenyl-C61-butyric acid methyl ester (PCBM, 99.5%) and bathocuproine (BCP, 99%) were all acquired from Xi'an Polymer Light Technology Corp. Nickel (II) nitrate hexahydrate ( $Ni(NO_3)_2 \cdot 6H_2O$ , 99%) was acquired from InnoChem, China. Nickel foil (300  $\mu$ m, 99.99%) was purchased from Shengshida metal materials Co., Ltd, China. Dimethyl sulfoxide (DMSO, 99.8%) and chlorobenzene (CB, 99.5%) were acquired from Sigma-Aldrich,  $\gamma$ -butyrolactone (GBL, 99.8%) were purchased from Aladdin. Ethyl alcohol (EtOH), isopropanol (IPA) and acetone were all purchased from Yonghua Chemical Technology (Jiangsu) Co., Ltd. China.

**Preparation of  $NiO_x$  Layer:** The patterned FTO/glass substrates were sequentially cleaned by sonication in acetone, IPA, EtOH, and deionized water for 15 min at each step. The ECD process for the  $NiO_x$  has been carried out in a two-electrode system, with the cleaned FTO/glass substrate as the working electrode, a nickel foil as the counter electrode and nickel (II) nitrate hexahydrate aqueous solution (0.02 M) as the electrolyte. The deposition was implemented using a constant current

density of 0.1 mA cm<sup>-2</sup> for 90 s controlled by a programmable electrochemical workstation (CS350H, Corrtest, China). Then the deposits were exposed to the UVO cleaning device (BZS250GF-TS, Hwotech, China) with different times and then annealed in a muffle furnace (Thermolyne, Thermo Scientific, USA) at 300 °C for 2 h. The control sample has been directly annealed under the same condition without UVO treatment.

**Device Fabrication:** Thereafter, the samples were transferred to a nitrogen-filled glovebox as the substrates to grow perovskite layer by one-step method. The perovskite precursor was prepared by dissolving 1 mMol of  $PbI_2$  and 1 mMol of  $CH_3NH_3I$  in 1 mL GBL and DMSO mixed solvent (7:3 v/v). This solution was spin-coated onto the  $NiO_x$  film at 500 rpm for 12 s and then 4000 rpm for 30 s. 150  $\mu$ L CB was rapidly dropped 10 s before the end of the spin-coating process. Subsequently, the samples were placed into an airtight glass pot and dried in the muffle furnace at 100 °C for 10 min. PCBM solution (20 mg/mL dissolved in CB) and BCP solution (0.5 mg mL<sup>-1</sup> in IPA) were then sequentially spun onto the perovskite layer at 2000 rpm for 30 s and 4000 rpm for 30 s, respectively. Each as-prepared solution has been filtered through a polytetrafluoroethylene (PTFE) filter (0.45  $\mu$ m) before spin-coating process. Finally, approximately 120 nm thick of silver electrodes were deposited on the top of BCP layer by thermal evaporation (PECVD350, Shenyang Xinlantian vacuum technology Co., Ltd, China). The active area of the PSC devices is 0.25 cm<sup>2</sup>.

**Characterization:** The morphology of the samples has been monitored by scanning electron microscopy (SEM, Carl Zeiss, Germany) and atomic force microscopy (AFM, Nanoscope IIIa Multimode, USA). Transmission spectra of the  $NiO_x$  HTL with and without UVO treatment were collected by UV/vis/NIR spectrophotometer (LAMBDA750, PerkinElmer, USA). The wettability of prepared  $NiO_x$  film was analyzed by a contact angle analyzer (DSA100, KRÜSS, Germany). The electrical performance of the UVO-treated and pristine  $NiO_x$  films was measured by a Keithley 2400 SourceMeter. The crystallinity of the samples has been characterized by X-ray diffraction (XRD, D8 ADVANCE, Germany). Furthermore, the elemental composition and energy band diagram of the prepared  $NiO_x$  films have been characterized by X-ray photoelectron spectroscopy (XPS, Thermo ESCALAB 250, USA) and ultraviolet photoelectron spectroscopy (UPS) using a monochromatic He-I light source with incident energy of 21.22 eV. The steady-state photoluminescence (PL) and time-resolved photoluminescence (TRPL) spectra of the samples have been measured by Steady-State & Time-Resolved Fluorescence Spectrofluorometer (QM/TM/IM, PTI, USA) with an excitation laser of 460 nm. The photocurrent density–voltage ( $J$ - $V$ ) curves of the as-fabricated devices have been measured under standard 1 sun AM 1.5G with a solar simulator (Newport, 2612A) in air, with the scanning rate at 0.1 V s<sup>-1</sup>. The solar simulator has been calibrated with a Newport 91150 V reference silicon cell system before measurement. The external quantum efficiency (EQE) spectra of PSCs have been measured using a quantum efficiency measurement system (QEX10, PV measurements, USA) in air without bias light. The electrochemical impedance spectroscopy (EIS) has been carried out at potentials of 0.7 V in the dark with frequencies sweeping from 1 Hz to 100 kHz by using an electrochemical workstation (CS350H, Corrtest, China) and the oscillation potential amplitudes were adjusted to 10 mV.

### Supporting Information

Supporting information is available from the Wiley Online Library or from the author.

### Acknowledgements

This work was supported by the Natural Science Foundation of China (11834011, 11674225, 11474201, and 11204176).

## Conflict of Interest

The authors declare no conflict of interest.

## Keywords

hole transport layer, nickel oxide, perovskite solar cells, ultraviolet-ozone treatment

Received: January 30, 2019

Revised: March 5, 2019

Published online: March 28, 2019

- [1] S. I. Seok, M. Gratzel, N. G. Park, *Small* **2018**, *14*, 1704177.
- [2] M. Saliba, J. P. Correa-Baena, M. Gratzel, A. Hagfeldt, A. Abate, *Angew. Chem. Int. Ed. Engl.* **2018**, *57*, 2554.
- [3] N. J. Jeon, H. Na, E. H. Jung, T.-Y. Yang, Y. G. Lee, G. Kim, H.-W. Shin, S. Il Seok, J. Lee, J. Seo, *Nat. Energy* **2018**, *3*, 682.
- [4] NREL. Efficiency chart. <https://www.nrel.gov/pv/assets/pdfs/pv-efficiency-chart.20190103.pdf> (accessed: January 2019).
- [5] Z. Wang, Q. Lin, B. Wenger, M. G. Christoforo, Y.-H. Lin, M. T. Klug, M. B. Johnston, L. M. Herz, H. J. Snaith, *Nat. Energy* **2018**, *3*, 855.
- [6] J. You, L. Meng, T. B. Song, T. F. Guo, Y. M. Yang, W. H. Chang, Z. Hong, H. Chen, H. Zhou, Q. Chen, *Nat. Nanotechnol.* **2016**, *11*, 75.
- [7] K. Lee, J. Ryu, H. Yu, J. Yun, J. Lee, J. Jang, *Nanoscale* **2017**, *9*, 16249.
- [8] J. Y. Jeng, K. C. Chen, T. Y. Chiang, P. Y. Lin, T. D. Tsai, Y. C. Chang, T. F. Guo, P. Chen, T. C. Wen, Y. J. Hsu, *Adv. Mater.* **2014**, *26*, 4107.
- [9] W. Chen, L. Xu, X. Feng, J. Jie, Z. He, *Adv. Mater.* **2017**, *29*, 1603923.
- [10] H. Rao, S. Ye, W. Sun, W. Yan, Y. Li, H. Peng, Z. Liu, Z. Bian, Y. Li, C. Huang, *Nano Energy* **2016**, *27*, 51.
- [11] P. Schulz, J. O. Tiepelt, J. A. Christians, I. Levine, E. Edri, E. M. Sanehira, G. Hodes, D. Cahen, A. Kahn, *ACS Appl. Mater. Inter.* **2016**, *8*, 31491.
- [12] W. Nie, H. Tsai, J. C. Blancon, F. Liu, C. C. Stoumpos, B. Traore, M. Kepenekian, O. Durand, C. Katan, S. Tretiak, J. Crochet, P. M. Ajayan, M. Kanatzidis, J. Even, A. D. Mohite, *Adv. Mater.* **2018**, *30*, 1703879.
- [13] X. Yin, Z. Yao, Q. Luo, X. Dai, Y. Zhou, Y. Zhang, Y. Zhou, S. Luo, J. Li, N. Wang, *ACS Appl. Mater. Inter.* **2017**, *9*, 2439.
- [14] W. Chen, Y. Zhou, L. Wang, Y. Wu, B. Tu, B. Yu, F. Liu, H. W. Tam, G. Wang, A. B. Djuricic, L. Huang, Z. He, *Adv. Mater.* **2018**, *30*, 1800515.
- [15] H. Zhang, J. Cheng, F. Lin, H. He, J. Mao, K. S. Wong, A. K. Jen, W. C. Choy, *ACS Nano* **2015**, *10*, 1503.
- [16] G. Li, Y. Jiang, S. Deng, A. Tam, P. Xu, M. Wong, H. S. Kwok, *Adv. Sci.* **2017**, *4*, 1700463.
- [17] S. Seo, I. J. Park, M. Kim, S. Lee, C. Bae, H. S. Jung, N. G. Park, J. Y. Kim, H. Shin, *Nanoscale* **2016**, *8*, 11403.
- [18] J. H. Park, J. Seo, S. Park, S. S. Shin, Y. C. Kim, N. J. Jeon, H. W. Shin, T. K. Ahn, J. H. Noh, S. C. Yoon, *Adv. Mater.* **2015**, *27*, 4013.
- [19] I. J. Park, G. Kang, M. A. Park, J. S. Kim, S. W. Seo, D. H. Kim, K. Zhu, T. Park, J. Y. Kim, *ChemSusChem* **2017**, *10*, 2660.
- [20] R. Islam, G. Chen, P. Ramesh, J. Suh, N. Fuchigami, D. Lee, K. A. Littau, K. Weiner, R. T. Collins, K. C. Saraswat, *ACS Appl. Mater. Inter.* **2017**, *9*, 17201.
- [21] Y. Wu, P. Wang, S. Wang, Z. Wang, B. Cai, X. Zheng, Y. Chen, N. Yuan, J. Ding, W. H. Zhang, *ChemSusChem* **2018**, *11*, 837.
- [22] Y. Chen, Z. Yang, S. Wang, X. Zheng, Y. Wu, N. Yuan, W. H. Zhang, S. F. Liu, *Adv. Mater.* **2018**, *30*, e1805660.
- [23] I. Jeong, H. Jung, M. Park, J. S. Park, H. J. Son, J. Joo, J. Lee, M. J. Ko, *Nano Energy* **2016**, *28*, 380.
- [24] L. Zuo, H. Guo, D. W. Dequillettes, S. Jariwala, M. N. De, S. Dong, R. Deblock, D. S. Ginger, B. Dunn, M. Wang, *Sci. Adv.* **2017**, *3*, e1700106.
- [25] R. Azmi, W. T. Hadmojo, S. Sinaga, C.-L. Lee, S. C. Yoon, I. H. Jung, S.-Y. Jang, *Adv. Energy Mater.* **2018**, *8*, 1701683.
- [26] Z.-L. Tseng, L.-C. Chen, C.-H. Chiang, S.-H. Chang, C.-C. Chen, C.-G. Wu, *Sol. Energy* **2016**, *139*, 484.
- [27] Q. Jiang, X. Zhang, J. You, *Small* **2018**, *14*, 1801154.
- [28] Z. Zhai, X. Huang, M. Xu, J. Yuan, J. Peng, W. Ma, *Adv. Energy Mater.* **2013**, *3*, 1614.
- [29] F. Wang, G. Sun, C. Li, J. Liu, S. Hu, H. Zheng, Z. Tan, Y. Li, *ACS Appl. Mater. Inter.* **2014**, *6*, 9458.
- [30] A. C. Sonavane, A. I. Inamdar, P. S. Shinde, H. P. Deshmukh, R. S. Patil, P. S. Patil, *J. Alloys Compd.* **2010**, *489*, 667.
- [31] J. Li, W. Zhao, F. Huang, A. Manivannan, N. Wu, *Nanoscale* **2011**, *3*, 5103.
- [32] M. Tyagi, M. Tomar, V. Gupta, *J. Mater. Res.* **2013**, *28*, 723.
- [33] M. S. Wu, H. H. Hsieh, *Electrochim. Acta* **2008**, *53*, 3427.
- [34] K. Yao, F. Li, Q. He, X. Wang, Y. Jiang, H. Huang, A. K. Y. Jen, *Nano Energy* **2017**, *40*, 155.
- [35] S. S. Mali, H. Kim, H. H. Kim, E. S. Sang, K. H. Chang, *Mater. Today* **2018**, *21*, 483.
- [36] D. Abubakar, N. Mahmoud Ahmed, S. Mahmud, N. Z. Alhazeem, *J. Nano Res* **2017**, *49*, 75.
- [37] J. He, E. Bi, W. Tang, Y. Wang, Z. Zhou, X. Yang, H. Chen, L. Han, *Sol. RRL* **2018**, *2*, 1800004.
- [38] A. Monshi, M. R. Foroughi, M. R. Monshi, *World J. Nano Sci. Eng.* **2012**, *02*, 154.
- [39] X. Yin, P. Chen, M. Que, Y. Xing, W. Que, C. Niu, J. Shao, *ACS Nano* **2016**, *10*, 3630.
- [40] T. Wang, D. Ding, X. Wang, R. Zeng, H. Liu, W. Shen, *ACS Omega* **2018**, *3*, 18434.
- [41] M. B. Islam, M. Yanagida, Y. Shirai, Y. Nabetani, K. Miyano, *ACS Omega* **2017**, *2*, 2291.
- [42] X. Yin, M. Que, Y. Xing, W. Que, *J. Mater. Chem. A* **2015**, *3*, 24495.
- [43] Y. Wu, F. Xie, C. Han, X. Yang, H. Su, M. Cai, Z. Zhou, T. Noda, L. Han, *Adv. Mater.* **2017**, *29*, 1701073.
- [44] C. O'Connell, R. Sherlock, M. D. Ball, B. Aszalós-Kiss, U. Prendergast, T. J. Glynn, *Appl. Surf. Sci.* **2009**, *255*, 4405.
- [45] F. Truica-Marasescu, S. Guimond, P. Jedrzejowski, M. R. Wertheimer, *Nucl. Instrum. Methods Phys. Res. B* **2005**, *236*, 117.
- [46] M.-R. Ahmadian-Yazdi, A. Rahimzadeh, Z. Chouqi, Y. Miao, M. Eslamian, *AIP Adv.* **2018**, *8*, 025109.
- [47] Y. Miao, P. Du, Z. Wang, Q. Chen, M. Eslamian, *Mater. Res. Express* **2018**, *5*, 026404.
- [48] J. Zheng, L. Hu, J. S. Yun, M. Zhang, C. F. J. Lau, J. Bing, X. Deng, Q. Ma, Y. Cho, W. F. Fu, *ACS Appl. Energy Mater.* **2018**, *1*, 561.
- [49] Y. Guo, X. Yin, J. Liu, W. Chen, S. Wen, M. Que, Y. Tian, Y. Yang, W. Que, *J. Adv. Dielectr.* **2018**, *08*, 1850006.
- [50] S. Park, S. Y. Kim, Y. Choi, M. Kim, H. Shin, J. Kim, W. Choi, *ACS Appl. Mater. Inter.* **2016**, *8*, 11189.
- [51] J. Cao, H. Yu, S. Zhou, M. Qin, T. K. Lau, X. Lu, N. Zhao, C. P. Wong, *J. Mater. Chem. A* **2017**, *5*, 11071.
- [52] S. Mu, D. Wu, Y. Wang, Z. Wu, X. Yang, W. Yang, *ACS Appl. Mater. Inter.* **2010**, *2*, 111.
- [53] X. Xu, Y. Yu, *Surf. Interface Anal.* **2002**, *33*, 343.
- [54] E. L. Ratcliff, J. Meyer, K. X. Steirer, A. Garcia, J. J. Berry, D. S. Ginley, D. C. Olson, A. Kahn, N. R. Armstrong, *Chem. Mater.* **2011**, *23*, 4988.
- [55] L. M. Mancieru, P. Colson, A. Maho, G. Eppe, N. D. Nguyen, C. Labrugere, A. Rougier, R. Cloots, C. Henrist, *J. Phys. D: Appl. Phys.* **2017**, *50*, 225501.
- [56] X. Yan, J. Zheng, L. L. Zheng, G. Lin, H. Lin, G. Chen, B. Du, F. Zhang, *Mater. Res. Bull.* **2018**, *103*, 150.

- [57] T. Leijtens, S. D. Stranks, G. E. Eperon, R. Lindblad, E. M. J. Johansson, I. J. Mcpherson, H. Rensmo, J. M. Ball, M. M. Lee, H. J. Snaith, *ACS Nano* **2014**, *8*, 7147.
- [58] S. Bag, M. F. Durstock, *ACS Appl. Mater. Inter.* **2016**, *8*, 5053.
- [59] G. Yang, C. Wang, H. Lei, X. Zheng, P. Qin, L. Xiong, X. Zhao, Y. Yan, G. Fang, *J. Mater. Chem. A* **2017**, *5*, 1658.
- [60] W. Ke, G. Fang, J. Wan, T. Hong, Q. Liu, L. Xiong, P. Qin, J. Wang, H. Lei, G. Yang, *Nat. Commun.* **2015**, *6*, 6700.
- [61] D. Yang, R. Yang, K. Wang, C. Wu, X. Zhu, J. Feng, X. Ren, G. Fang, S. Priya, S. F. Liu, *Nat. Commun.* **2018**, *9*, 3239.
- [62] M. Jones, S. S. Lo, G. D. Scholes, *J. Phys. Chem. C* **2017**, *113*, 18632.
- [63] M. Wang, B. Li, P. Siffalovic, L.-C. Chen, G. Cao, J. Tian, *J. Mater. Chem. A* **2018**, *6*, 15386.
- [64] Z. Q. Huang, X. T. Hu, C. Liu, L. C. Tan, Y. W. Chen, *Adv. Funct. Mater.* **2017**, *27*, 1703061.
- [65] W. Chen, Y. Wu, Y. Yue, J. Liu, W. Zhang, X. Yang, H. Chen, E. Bi, I. Ashrafali, M. Grätzel, *Science* **2015**, *350*, 944.
- [66] L. J. Tang, X. Chen, T. Y. Wen, S. Yang, J. J. Zhao, H. W. Qiao, Y. Hou, H. Yang, *Chem. – Eur. J.* **2018**, *24*, 2845.
- [67] T. Niu, J. Lu, R. Munir, J. Li, D. Barrit, X. Zhang, H. Hu, Z. Yang, A. Amassian, K. Zhao, S. F. Liu, *Adv. Mater.* **2018**, *30*, 1706576.
- [68] A. Huang, L. Lei, J. Zhu, Y. Yu, Y. Liu, S. Yang, S. Bao, X. Cao, P. Jin, *ACS Appl. Mater. Inter.* **2017**, *9*, 2016.
- [69] W. E. I. Sha, X. Ren, L. Chen, W. C. H. Choy, *Appl. Phys. Lett.* **2015**, *106*, 221104.
- [70] P. Lopez-Varo, J. A. Jiménez-Tejada, M. García-Rosell, S. Ravishankar, G. Garcia-Belmonte, J. Bisquert, O. Almora, *Adv. Energy Mater.* **2018**, *8*, 1702772.
- [71] X. Zhou, Y. Zhang, W. Kong, M. Hu, L. Zhang, C. Liu, X. Li, C. Pan, G. Yu, C. Cheng, B. Xu, *J. Mater. Chem. A* **2018**, *6*, 3012.
- [72] Y. Li, B. Ding, Q. Q. Chu, G. J. Yang, M. Wang, C. X. Li, C. J. Li, *Sci. Rep.* **2017**, *7*, 46141.
- [73] T. H. Liu, K. Chen, Q. Hu, R. Zhu, Q. H. Gong, *Adv. Energy Mater.* **2016**, *6*, 1600457.
- [74] A. S. Chouhan, N. P. Jasti, S. Avasthi, *Mater. Lett.* **2018**, *221*, 150.
- [75] J. Zhang, H. Luo, W. Xie, X. Lin, X. Hou, J. Zhou, S. Huang, W. Ou-Yang, Z. Sun, X. Chen, *Nanoscale* **2018**, *10*, 5617.
- [76] C. Bi, Q. Wang, Y. Shao, Y. Yuan, Z. Xiao, J. Huang, *Nat. Commun.* **2015**, *6*, 7747.
- [77] Y. Hou, X. Du, S. Scheiner, D. P. McMeekin, Z. Wang, N. Li, M. S. Killian, H. Chen, M. Richter, I. Levchuk, *Science* **2017**, *358*, 1192.
- [78] W. Q. Wu, D. Chen, Y. B. Cheng, R. A. Caruso, *Sol. RRL* **2017**, *1*, 1700117.
- [79] D. H. Kim, J. Park, Z. Li, M. Yang, J. S. Park, I. J. Park, J. Y. Kim, J. J. Berry, G. Rumbles, K. Zhu, *Adv. Mater.* **2017**, *29*, 1606831.
- [80] M. M. Tavakoli, S. M. Zakeeruddin, M. Gratzel, Z. Fan, *Adv. Mater.* **2018**, *30*, 1705998.
- [81] R. Kang, J. S. Yeo, H. J. Lee, S. Lee, M. Kang, N. Myoung, S. Y. Yim, S. H. Oh, D. Y. Kim, *Nano Energy* **2016**, *27*, 175.
- [82] D. Yang, R. Yang, J. Zhang, Z. Yang, S. Liu, C. Li, *Energ. Environ. Sci.* **2015**, *8*, 3208.
- [83] Y. K. Ren, X. Q. Shi, X. H. Ding, J. Zhu, T. Hayat, A. Alsaedi, L. I. Zhaoqian, X. X. Xu, S. Yang, S. Dai, *Inorg. Chem. Front.* **2017**, *5*, 348.
- [84] M. A. Mahmud, N. K. Elumalai, M. B. Upama, D. Wang, K. H. Chan, M. Wright, C. Xu, F. Haque, A. Uddin, *Sol. Energy Mater. Sol. Cells* **2017**, *159*, 251.
- [85] L. Yang, M. Wu, F. Cai, P. Wang, R. S. Gurney, D. Liu, J. Xia, T. Wang, *J. Mater. Chem. A* **2018**, *6*, 10379.
- [86] W. Tress, A. Merten, M. Furno, M. Hein, K. Leo, M. Riede, *Adv. Energy Mater.* **2013**, *3*, 631.
- [87] L. Wu, H. Zang, Y. C. Hsiao, X. Zhang, B. Hu, *Appl. Phys. Lett.* **2014**, *104*, 1300864.
- [88] V. N. Bliznyuk, J. Gasiorowski, A. A. Ishchenko, G. V. Bulavko, M. Rahaman, K. Hingerl, D. R. T. Zahn, N. S. Sariciftci, *Appl. Surf. Sci.* **2016**, *389*, 419.
- [89] P. Loper, M. Stuckelberger, B. Niesen, J. Werner, M. Filipic, S. J. Moon, J. H. Yum, M. Topic, S. De Wolf, C. Ballif, *J. Phys. Chem. Lett.* **2015**, *6*, 66.
- [90] M. P. de Haas, J. M. Warman, T. D. Anthopoulos, D. M. de Leeuw, *Adv. Funct. Mater.* **2006**, *16*, 2274.